JOURNAL OF THEORETICAL AND APPLIED MECHANICS
62, 4, pp. 827-839, Warsaw 2024
https://doi.org/10.15632/jtam-pl/193952

PREDICTION AND MITIGATION OF INSTABILITY IN ULTRA LONG DRILLING SHAFT LINING STRUCTURES USING THE CUSP CATASTROPHE MODEL

Jimin Liu, Ruixue Pan, Hua Cheng, Haixu Fan

School of Civil Engineering and Architecture, Anhui University of Science and Technology, Huainan, China; and State Key Laboratory of Mining Response and Disaster Prevention and Control in Deep Coal Mine, Huainan, China
corresponding author J.M. Liu, e-mail: jimliu@aust.edu.cn

This paper deals with the stability prediction of an ultralong drilling shaft lining structure and how to mitigate its structural instability. Based on catastrophic characteristics of the instability process, the catastrophe method and a cusp catastrophic model is applied in analyzing the instability optimization measure. The process and mechanism of catastrophe instability is analyzed, and its corresponding instability criterion is founded. A case study and numerical results show that this optimization measure can increase its critical depth by 45% and mitigate structural vertical instability, which provides a theoretical possibility for the stability control technology of ultra long shaft lining structures.

Keywords: cusp catastrophic model, critical depth, instability criterion, drilling shaft lining structure

1. Introduction

A shaft drilling method is a special construction method in coal and copper mine constructions all over the world, which is also used in subways and municipal engineering (Liu and Meng, 2015; Dorn and Kaledin, 2013; Hara *et al.*, 2019). In drilling shaft lining structures (DSLS) during its construction, buckling usually becomes a dominated failure pattern rather than damage due to material strength, which is often related to deformation of the whole DSLS experiencing a sudden and irreversible change when it reaches or exceeds the critical value. Any slight eccentricity or lateral force can cause shaft lining to suddenly tilt and slip, resulting in vertical instability of DSLS. Moreover, the longer the construction length of DSLS, the greater the possibility of vertical instability of the structure. Stability characteristics of DSLS have become a problem in shaft construction and seriously restricted its application in the deep coal mine shaft engineering. Therefore, it is necessary to take measures to predict and suppress the vertical instability of DSLS in ultra long coal mines and carry out corresponding theoretical research.

At present, many scholars have conducted numerous researches on stability characteristics of shaft lining structures. Most of them regarded DSLS as a slender compression rod hinged at both ends when it is sunk to the bottom of the well and before cementing and filling, and analyzed stability of the structure based on the energy method (Wegner and Kurpisz, 2017; Xing *et al.*, 2023). Hong (1980) initially mentioned that there exists a structural instability with DSLS and suggested adding counterweight water to control the instability. Niu *et al.* (2006) believed that the counterweight water should be regarded as lateral pressure and established a critical depth calculation method in constant cross-section DSLS. Cheng *et al.* (2008) used the same mechanical background and proposed the critical depth of variable cross-section DSLS. They all raised their instability criterion and critical depth based on the principle of minimum potential energy. Their research results have been well verified and applied in shaft engineering

at a depth of 600m. But the studies on predicting the vertical instability of ultra long DSLS with a construction depth exceeding 600m and the mitigating instability optimization measure is scare.

Furthermore, there are many studies concerning catastrophe theory and its application. Catastrophe theory is a fundamental method of scientific research, which uses mathematical models to explain various forms and structures of discontinuous catastrophe phenomena. It has many successful application examples in many disciplines such as stability of elastic structures, economy and natural science (Merli and Pavese, 2018; Karman and Pawlowski, 2019; Niu *et al.*, 2023). Especially in the field of civil engineering, catastrophe theory has helped to solve many problems such as the critical buckling load of pile foundation, soil slope and etc. (Lei *et al.*, 2022; Xu and Ni, 2019). Liu *et al.* (2020, 2022) established a catastrophe model for the instability of DSLS and analyzed its instability mechanics under THE traditional construction method. It can be found that the studies on catastrophe theory and its catastrophic models can help one to solve structural instability problems and have ideal application effects.

Motivated by this, this paper proposes a cusp catastrophic model based on catastrophe theory to reveal the characteristic of an ultra long shaft structure instability phenomenon when using instability optimization measures. Based on abrupt and irreversible characteristics during the instability process, the catastrophe method and a cusp catastrophic model was applied. Firstly, an instability optimization measure is proposed and a cusp catastrophe model is established. Based on the catastrophe method and catastrophic model, the instability characteristics of ultra long DSLS is analyzed. In the end, the critical depth affecting factors are discussed, and an actual engineering verifies the effectiveness of the instability optimization measure.

2. Theoretical model

2.1. Instability optimization measures in ultra long drilling shaft lining

In general, the traditional construction of the shaft drilling method concludes three steps: suspending and sinking the shaft, suspended and sunks to the bottom of the well but not yet filled and cemented, and filled cemented the shaft. Figure 1a shows a schematic representation and a scene diagram of the shaft construction during suspension and subsidence. When the last prefabricated shaft segments finish its connection, the whole DSLS lands on the bedrock directly. The moment when the shaft floats and sinks to the bottom and touches the bottom of the well on the bedrock but not yet filled and cemented, the horizontal and vertical displacement at the bottom of DSLS is limited and forms a bi-directional hinged support. At the same time the shaft is controlled by guided wood for lateral displacement at the wellhead position. The two ends of the entire DSLS are hinged and constrained. And geometric dimensions in the vertical direction are significantly higher than those in the horizontal direction, thus forming a slender rod with both ends hinged. At this moment, any slight eccentricity or lateral force during construction may cause structural sloping or sliding, resulting in overall instability of DSLS.

To improve the overall structural stability of DSLS in the ultra long coal mine shaft engineering, we propose the instability optimization measures of pre pouring cement slurry before the shaft touches the bottom. Before the shaft is suspended and sinks to the bottom of the well, cement mortar is injected into the well through a grouting pipe in advance. The speed of suspension and sinking of the shaft is controlled by controlling the injection amount and speed of counterweight water, so that the shaft is slowly embedded into the bottom of the well. 4-6 grouting pipes are evenly arranged around the well, with diameters ranging from 50 mm to 250 mm and a length equal to depth of the shaft. The grouting pipe gradually increases as the cement mortar level rises and is removed from the top. Figure 1b shows a schematic representation and a scene diagram of the instability optimization measure. Through applying this optimization

measure, the bottom of the shaft is fixed. The constraint manner at the bottom is intervened and optimized from hinged to fixed.

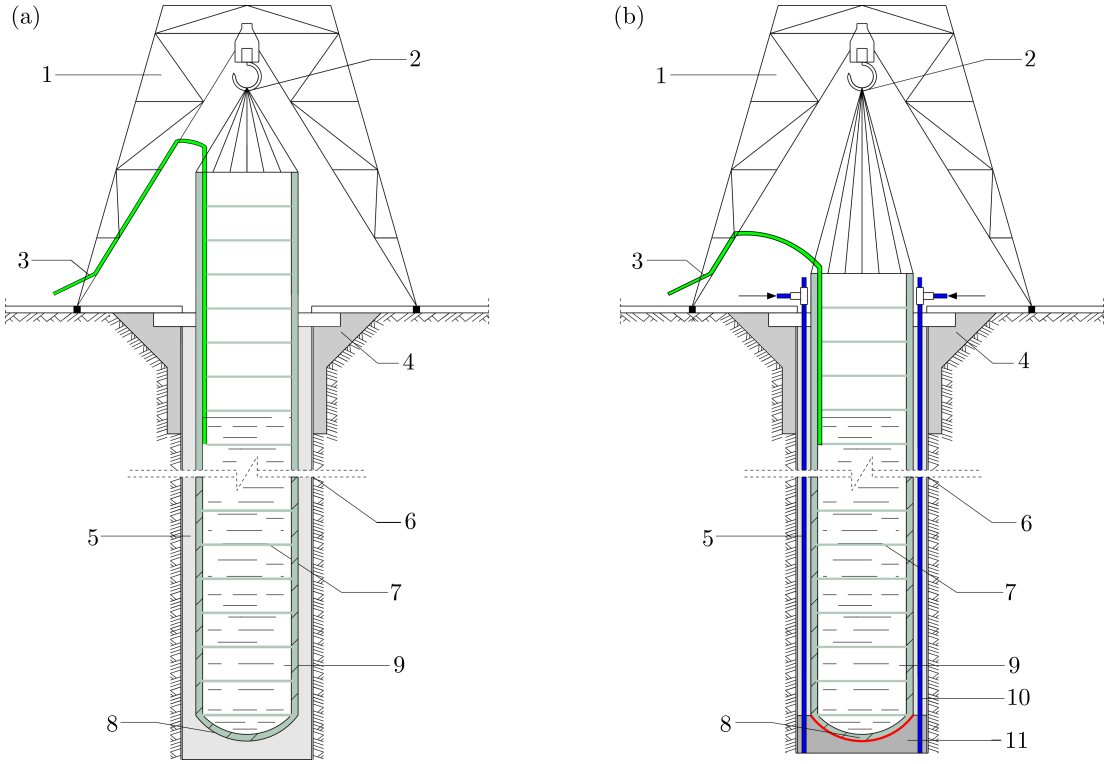

Fig. 1. Schematic representation and the scene diagram of the shaft drilling method: (a) traditional construction measure, (b) instability optimization measure; 1 – gantry crane, 2 – drilling platform, 3 – main water pipe, 4 – guided wood at wellhead, 5 – mud, 6 – well holes, 7 – shaft segment, 8 – shaft lining bottom, 9 – counterweight water, 10 – pumping pipe of cement slurry, 11 – cement slurry

2.2. Basic assumption and mechanical background

For convenience of the discussion, we assume that the inner diameter of the shaft remains unchanged and the shaft material is described by a single specification. The counterweight water level has not reached the wellhead position. Furthermore, we make the following basic assumptions:

Assumption 1. The shaft material is linearly elastic and follows Hooke's law.

Assumption 2. DSLS can be regarded as a slender rod with the bottom fixed and top hinged, and its deflection curve equation satisfies $y = \delta[\cos(3\pi x/2H) - \cos(\pi x/2H)]$, where δ is the maximum displacement of deflection curve, H is height of the shaft structure (Yang, 2019).

Assumption 3. DSLS obeys the theory of small deflection of structural stability (Ozbasaran, 2018). The rod has no initial defects or stresses. During buckling, the rod only undergoes planar bending deformation, and the bending deformation is small.

The force acting on DSLS includes the self-weight of shaft P_c, the lateral pressure of mud on the outer surface of shaft P_m, the lateral pressure of counterweight water on the inner surface of shaft P_w, the reverse force on the top of shaft R_B, and the reverse force on the bottom of the shaft R_A, which is shown in Fig. 2a.

The lateral pressure caused by the mud unit length on the outer surface of shaft p_m can be expressed as $p_m = (1/4)\pi D^2 \gamma_m \sin\alpha$. D is outer diameter of the shaft, γ_m is weight of mud, α is inclination of the deflection curve. The force direction is along the normal direction of the deflection curve. The lateral pressure caused by unit length counterweight water on the inner surface of shaft p_w can be expressed as $p_w = (\pi/4)d^2\gamma_w \sin\alpha$. d is inner diameter of the shaft, γ_w is weight of water. Its force direction is also along the normal direction of the deflection curve. The self-weight of the reinforced concrete shaft per unit length is $p_c = (\pi/4)(D^2 - d^2)[\gamma_c(1-\rho)+\gamma_s\rho]$. γ_c and γ_s are weights of concrete and steel, ρ is the reinforcement ratio of the reinforced concrete shaft. The direction is vertical downwards. Due to the absence of displacement at supports A and B, the external force potential energy generated by R_A and R_B is 0. We will not discuss the reverse force on the bottom of the shaft R_A and the reverse force on the top of the shaft R_B. Based on Assumption 2 and the mechanics of background, the deformation deflection curve and stability analysis calculation diagram of DSLS after using the instability optimization measure can be obtained, as shown in Fig. 2b.

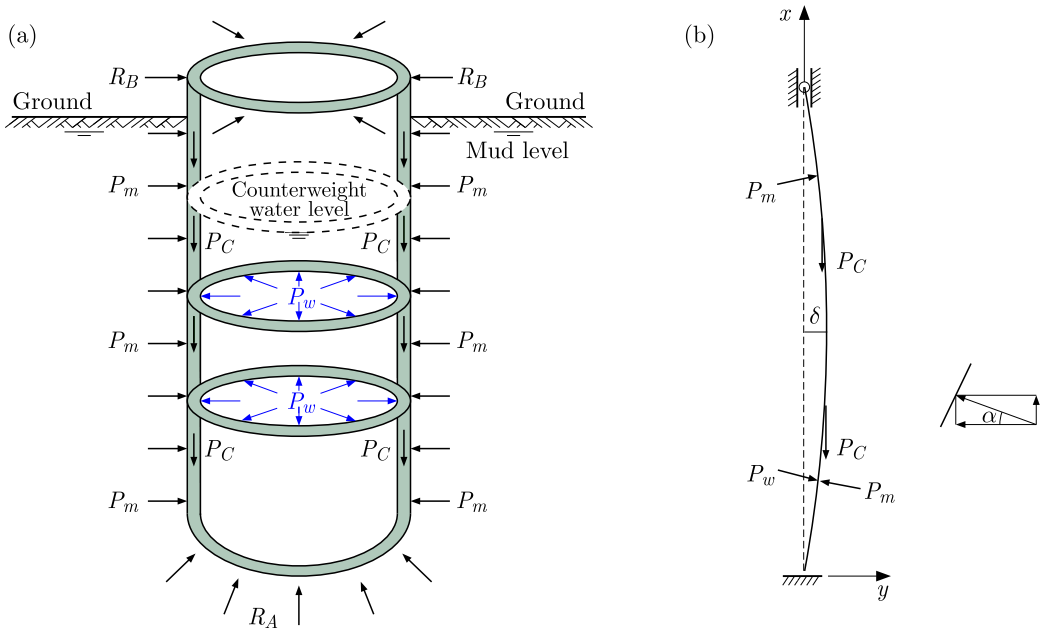

Fig. 2. Force and stability analysis of the shaft by using the instability optimization measure: (a) force analysis of shaft, (b) schematic diagram of stability analysis

2.3. Total potential energy equation

The total potential energy Π of DSLS is the sum of strain energy U released by the vertical bending deformation of the structure and external force potential energy V, expressed as

$$\Pi = U + V \tag{2.1}$$

According to Assumption 3, DSLS obeys the theory of small deflection of structural stability. In curvature equation $1/\rho = y''/\sqrt{(1+y'^2)^3}$, compared to 1, y'^2 can be ignored, the curvature can be approximated by y''. The in-plane bending moment can expressed as $M = 1/\rho = y''$. Based on the deflection curve equation in Assumption 2, the total strain energy of DSLS is

$$U = \int_0^H \frac{M^2}{2EI}\,dx = \frac{1}{2}\int_0^H EIy''^2\,dx = \frac{41EI\pi^4}{32H^3}\delta^2 \tag{2.2}$$

The external force potential energy V acting on the system is the total of external force potential energy V_y caused by the vertical force P and external force potential energy V_x caused by the horizontal force. V_y can be determined by $V_y = -p\lambda$, where λ is small deformation generated by the system under vertical force p. According to Assumption 3, the small deformation satisfies $\lambda = d_s - d_x = y'^2 d_x/4$. On the other hand, the external force potential energy V_x caused by the vertical force includes external force potential energy caused by horizontal component of mud lateral pressure $(V_m)_x$ and external force potential energy caused by the horizontal component of counterweight water pressure $(V_w)_x$. So the external force potential energy can be expressed as

$$\begin{aligned} V = V_y + V_x = &-P_c\lambda_c - (P_m)_y\lambda_m(P_w)_y\lambda_w + (V_w)_x + (V_m)_x = \Big(\frac{1-5}{16}\pi^2\Big)p_c\delta^2 \\ &+ \frac{\pi^3 D^2\gamma_m}{4}\Big(\frac{183\pi^2}{256H^2} + \frac{308}{75}\Big)\delta^4 - \frac{\pi d^2\gamma_w}{2}\sin^2\frac{\pi H_w}{2H}\sin^2\frac{\pi H_w}{H}\delta^2 + Q_m\delta \\ &- \frac{\pi^5 d^2\gamma_w\delta^4}{128H^2}\Bigg\{ - \frac{1}{\pi^2}\Big[\frac{17657}{1200}\cos\frac{\pi H_w}{H} - \frac{9913}{600}\cos\frac{2\pi H_w}{H} \\ &+ 9\Big(-\frac{1267}{120} + \frac{549}{1200}\cos\frac{3\pi H_w}{H} + \frac{1}{100}\cos\frac{4\pi H_w}{H} + \frac{1}{8}\cos\frac{5\pi H_w}{H}\Big)\Big]\sin^2\frac{\pi H_w}{2H} \\ &+ \frac{15}{\pi}\Big(- \frac{59}{15}\sin\frac{\pi H_w}{H} + \frac{83}{48}\sin\frac{2\pi H_w}{H} - \frac{37}{30}\sin\frac{3\pi H_w}{H} + \frac{27}{80}\sin\frac{4\pi H_w}{H} \\ &- \frac{9}{50}\sin\frac{5\pi H_w}{H} + \frac{9}{80}\sin\frac{6\pi H_w}{H}\Big)\frac{H_w}{H} + \frac{183}{8}\Big(\frac{H_w}{H}\Big)^2\Bigg\} \end{aligned} \tag{2.3}$$

Take

$$\begin{aligned} A_1 = &-\frac{1}{\pi^2}\Big[\frac{17657}{1200}\cos\frac{\pi H_w}{H} - \frac{9913}{600}\cos\frac{2\pi H_w}{H} + 9\Big(-\frac{1267}{120} + \frac{549}{1200}\cos\frac{3\pi H_w}{H} \\ &+ \frac{1}{100}\cos\frac{4\pi H_w}{H} + \frac{1}{8}\cos\frac{5\pi H_w}{H}\Big)\Big]\sin^2\frac{\pi H_w}{2H} + \frac{15}{\pi}\Big(-\frac{59}{15}\sin\frac{\pi H_w}{H} + \frac{83}{48}\sin\frac{2\pi H_w}{H} \\ &- \frac{37}{30}\sin\frac{3\pi H_w}{H} + \frac{27}{80}\sin\frac{4\pi H_w}{H} - \frac{9}{50}\sin\frac{5\pi H_w}{H} + \frac{9}{80}\sin\frac{6\pi H_w}{H}\Big)\frac{H_w}{H} + \frac{183}{8}\Big(\frac{H_w}{H}\Big)^2 \end{aligned} \tag{2.4}$$

By substituting formulas (2.2)-(2.4) into (2.1), we obtain the total potential energy function

$$\begin{aligned} \Pi = &\Big[-\frac{A_1\pi^5 d^2\gamma_w}{128H^2} + \frac{\pi^3 D^2\gamma_m}{4}\Big(\frac{183\pi^2}{256H^2} + \frac{308}{75}\Big)\Big]\delta^4 \\ &+ \Big(\frac{41EI\pi^4}{32H^3} + \frac{1-5}{16}\pi^2\Big)p_c - \frac{\pi d^2\gamma_w}{2}\sin^2\frac{\pi H_w}{2H}\sin^2\frac{\pi H_w}{H}\Big)\delta^2 + Q_m\delta \end{aligned} \tag{2.5}$$

2.4. A cusp catastrophic model for DSLS

Do equivalent transformation on (2.5), if

$$\begin{aligned} A_2 &= -\frac{A_1\pi^5 d^2\gamma_w}{128H^2} + \frac{\pi^3 D^2\gamma_m}{4}\Big(\frac{183\pi^2}{256H^2} + \frac{08}{75}\Big) \\ A_3 &= \frac{41EI\pi^4}{32H^3} + \Big(\frac{1-5}{16\pi^2}\Big)p_c - \frac{\pi d^2\gamma_w}{2}\sin^2\frac{\pi H_w}{2H}\sin^2\frac{\pi H_w}{H} \\ A_4 &= Q_m = \int_0^H p_m\cos\alpha\ d_x = 0 \end{aligned} \tag{2.6}$$

Meanwhile, the dimensionless parameters x, m and n are introduced as $x = 4\sqrt{4A_2}\delta$, $m = A_3/\sqrt{A_2}$, $n = A_4/\sqrt[4]{4A_2}$. The total potential energy function of DSLS can be expressed as

$$\Pi(x) = \frac{1}{4}x^4 + \frac{1}{2}mx^2 + nx \tag{2.7}$$

This equation has two control variables m and n, and one state variable x. According to Thom's classification theorems (Pacoste, 1993), DSLS conforms to the cusp catastrophe mathematical model (Li *et al.*, 2016).

Let the first derivative of the total potential function be zero

$$\Pi'(x) = x^3 + mx + n = 0 \tag{2.8}$$

The pints that satisfy equation (2.8) are critical points. But a critical point may not necessarily be a stable point, it may make the system stable or unstable. Only the point where the potential function takes a unique extremum is a stable point. So in order to make the structure stable, it is necessary to simultaneously satisfy the equation

$$\Pi''(x) = 3x^2 + m = 0 \tag{2.9}$$

Combine equations (2.8) and (2.9) to obtain the bifurcation set equation

$$\Delta = 4m^3 + 27n^2 = 0 \tag{2.10}$$

The points that satisfy equation (2.10) form the singularity set S. The projection of singularity set S in control variable plane C is called the bifurcation points set B. Figure 3 shows the singularity set S, bifurcation point set B and equilibrium surface M of the cusp catastrophe model (Saunders, 1980). The equilibrium surface M is made of all critical points that fulfill equation (2.8). M is a well-known surface made up of the control variables m and n and the state variables x.

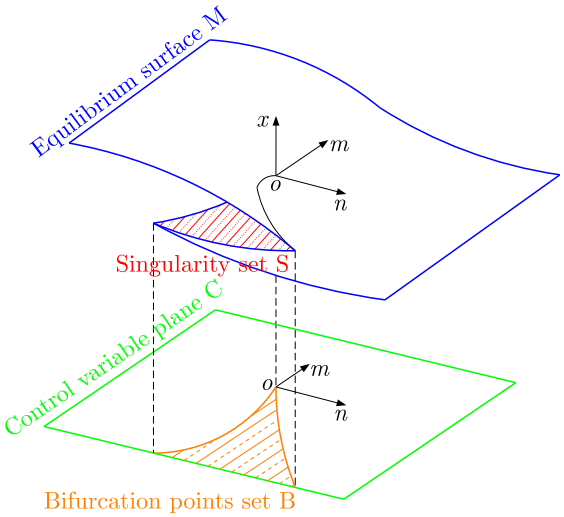

Fig. 3. Diagram of the equilibrium surface and the bifurcation set of cusp catastrophe model

3. Analysis and discussion

3.1. Catastrophic instability analysis

As the total potential energy function of DSLS conforms to the cusp catastrophe model, it will be analyzed by the cusp catastrophe model. In the cusp catastrophic model, the values of control variables m and n directly determine the stable state of the shaft. It is only when the equilibrium point crosses the bifurcation points set B when there is a possibility of vertical instability. The bifurcation set equation composed of control variables is the key to determining system instability (Saunders, 1980; Zhao *et al.*, 2023). When $\Delta > 0$, the control variables (m, n)

fall outside the bifurcation points set B, the system is located on the upper and lower leaves of the equilibrium surface M, the system (here refers to ultralong DSLS) is in a stable equilibrium state. When $\Delta < 0$, the control variables (m, n) fall within the bifurcation points set B, the system is located in the middle of the equilibrium surface M, and ultra long DSLS is in an unstable equilibrium state. When $\Delta = 0$, the control variables (m, n) fall on the boundary of the bifurcation points set B, the ultralong DSLS is in a critical stable equilibrium state.

The vertical instability and failure of ultralong DSLS is an evolutionary process from gradual to sudden changes. With a continuous connection of the shaft segment and the increasing injection of counterweight water into the shaft, the shaft structure begins to accumulate elastic potential energy. The total potential energy accumulated by the shaft structure maintains a stable equilibrium with dynamics and uncertainty. When the elastic potential energy of the shaft accumulates to a certain extent, the structure in a dynamic equilibrium state will induce structural instability by certain conditions.

3.2. Design of critical depth for instability and instability criterion of ultra long DSLS

Observe equations (2.6), as $A_4 = 0$, so $n = 0$ and

$$\Delta = 4m^3 = 4\Big(\frac{A_3}{\sqrt{A_2}}\Big)^3 = 4\left(\frac{\frac{41EI\pi^4}{32H^3} + \Big(1 - \frac{5}{16}\pi^2\Big)p_c - \frac{\pi d^2\gamma_w}{2}\sin^2\frac{\pi H_w}{2H}\sin^2\frac{\pi H_w}{H}}{\sqrt{-\frac{A_1\pi^5 d^2\gamma_w}{128H^2} + \frac{\pi^3 D^2\gamma_m}{4}\Big(\frac{183\pi^2}{256H^2} + \frac{308}{75}\Big)}}\right)^3 \tag{3.1}$$

When ultra long DSLS is in a critical stable equilibrium state, then the $\Delta = 0$. From Eq. (3.1) one can obtain the critical depth H_{cr} for instability of ultra long DSLS

$$H_{cr} = \sqrt[3]{\frac{41EI\pi^4}{(10\pi^2 - 32)p_c + 16\pi d^2\gamma_w \sin^2\frac{\pi H_w}{2H}\sin^2\frac{\pi H_w}{H}}} \tag{3.2}$$

When ultra long DSLS is in a stable equilibrium state, the $\Delta > 0$. From Eq. (3.1) one can find that the construction height of ultra long DSLS should satisfy

$$H < \sqrt[3]{\frac{41EI\pi^4}{(10\pi^2 - 32)p_c + 16\pi d^2\gamma_w \sin^2\frac{\pi H_w}{2H}\sin^2\frac{\pi H_w}{H}}} \tag{3.3}$$

On the right-hand side of inequality (3.3) there is just the critical depth H_{cr}, so inequality (3.3) can also be expressed as the relationship between construction height and critical depth $H < H_{cr}$.

When ultra long DSLS is in an unstable equilibrium state, the $\Delta < 0$. From Eq. (3.1) one can find that the construction height of ultra long DSLS should satisfy

$$H > \sqrt[3]{\frac{41EI\pi^4}{(10\pi^2 - 32)p_c + 16\pi d^2\gamma_w \sin^2\frac{\pi H_w}{2H}\sin^2\frac{\pi H_w}{H}}} \tag{3.4}$$

Simultaneously with Eq. (3.2), the instability conditions of ultra long DSLS can also be expressed as the relationship between construction height and critical depth $H > H_{cr}$.

Thus, the following can be used to convey ultra long DSLS instability criterion when applying the instability optimization measure

$$\begin{aligned} &H < H_{cr} && \text{ultra long DSLS is stable} \\ &H = H_{cr} && \text{ultra long DSLS is in critical instability} \\ &H > H_{cr} && \text{ultra long DSLS is unstable} \end{aligned} \tag{3.5}$$

3.3. Discussion of critical depth

In this part, a numerical study is conducted to investigate the influence effect of different factors on the critical depth. It can be seen from Eq. (3.2) that the factors affecting the critical depth include the shaft elastic modulus E, inertia moment I, inner diameter d, self-weight per unit length p_c and height of counterweight water H_w. But the shaft inertia moment is determined by the inner and outer diameters, while the outer diameter is generally a fixed value of 8 m or more, so the moment of inertia is determined by the inner diameter. The actual influence factors only contain E, d, p_c and H_w. Among them, E, d, p_c are the internal characteristics. H_w is the external factor. The process leading to the instability of ultra long DSLS when applying the instability optimization measure is a result of the combined action of its internal characteristics and external factors.

In ultra long shaft engineering, these four influence factors have a certain range. As the shaft segment is generally made of C35C̃80 concrete (Fang *et al.*, 2023), E ranges from 31.5 GPa to 38 GPa. The outside diameter of the shaft is often greater than 8 m. The thickness ranges from 500 mm to 850 mm according to the shaft strength requirement. So d ranges from 6.3 m to 7 m. p_c is related to the making method of the shaft segment. Generally, it is no less than $3 \cdot 10^5$ N/m. H_w is required to meet the shaft suspension and anti-overturning standards. The minimum and maximum heights of H_w is restricted. Usually, H_w will be greater than half of the shaft construction height. Here we choose three shaft construction heights, 650 m, 700 m and 750 m, and calculate the critical depth for fifteen independent variables within their reasonable range. The basic parameters are set to be $D = 8$ m, $d = 6.3$ m, $p_c = 3 \cdot 10^5$ N/m, $H_w = 380$ m. The critical depth with different elastic modulus is shown in Fig. 4a. The calculation results under three construction heights all show that the larger the elastic modulus, the greater the critical depth. And the critical depths are all greater than the corresponding construction height, the shaft is vertically stable. It illustrates that the use of high-strength materials is beneficial for improving the vertical stability of ultra long DSLS.

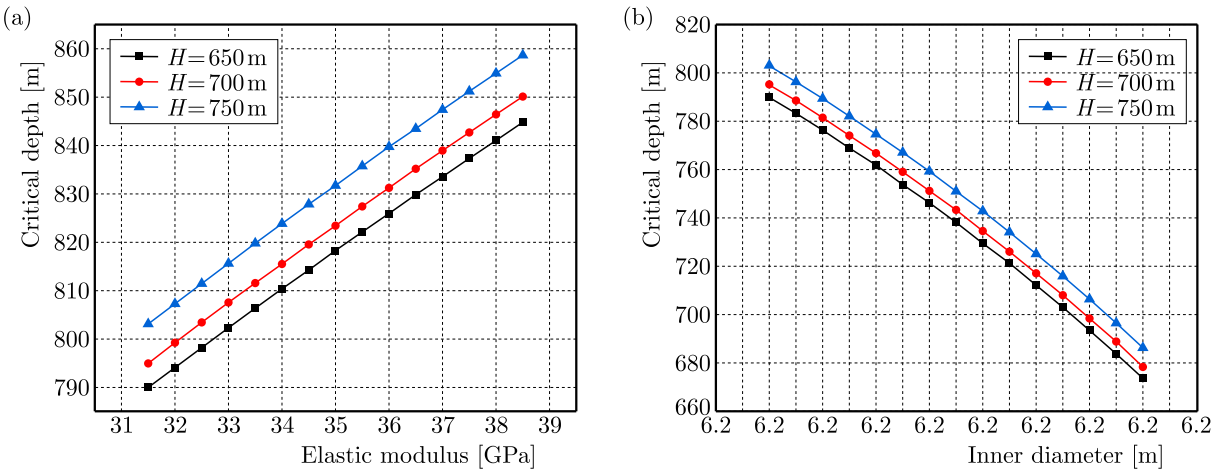

Fig. 4. Critical depth with different elastic moduli (a) and inner diameter (b) for three construction heights

Another investigation was devised to investigate the relationship between critical depth and inner diameter. When taking $E = 31.5$ GPa, other parameters are also set to be $D = 8$ m, $p_c = 3 \cdot 10^5$ N/m, $H_w = 380$ m. The critical depth with different inner diameters is shown in Fig. 4b. The calculation results under three construction heights all show that the smaller the inner diameter, the greater the critical depth. For the construction height of 650 m, the critical depth is greater than construction height and the shaft is vertically stable. But for the construction height of 700 m and 750 m, the critical depth is not always greater than construction

height and the structure may not necessarily be stable. Due to relatively fixed outer diameter in ultralong DSLS, the size of inner diameter is closely related to thickness of the shaft. It illustrates that using a smaller inner diameter or thicker shaft is more conducive to structural stability. When construction height exceeds 700 meters, it is necessary to control its inner diameter or thickness.

Another investigation was developed to explore the relationship between critical depth and unit length self-weight. When taking $D = 8\,\text{m}$, $d = 6.3\,\text{m}$, $E = 31.5\,\text{GPa}$, $H_w = 380\,\text{m}$, the critical depth with different unit length self-weight is shown in Fig. 5a. The calculation results under three construction heights all show that the larger the inner diameter, the smaller the critical depth. For the construction height of 650 m, the critical depth is greater than construction height and the structure is vertically stable. But for the construction height of 700 m and 750 m, the critical depth is not always greater than construction height and the structure may not necessarily be stable. It suggests that using a lightweight shaft material is more conducive to structural stability. When construction height exceeds 700 meters, controlling its unit length self-weight is critical.

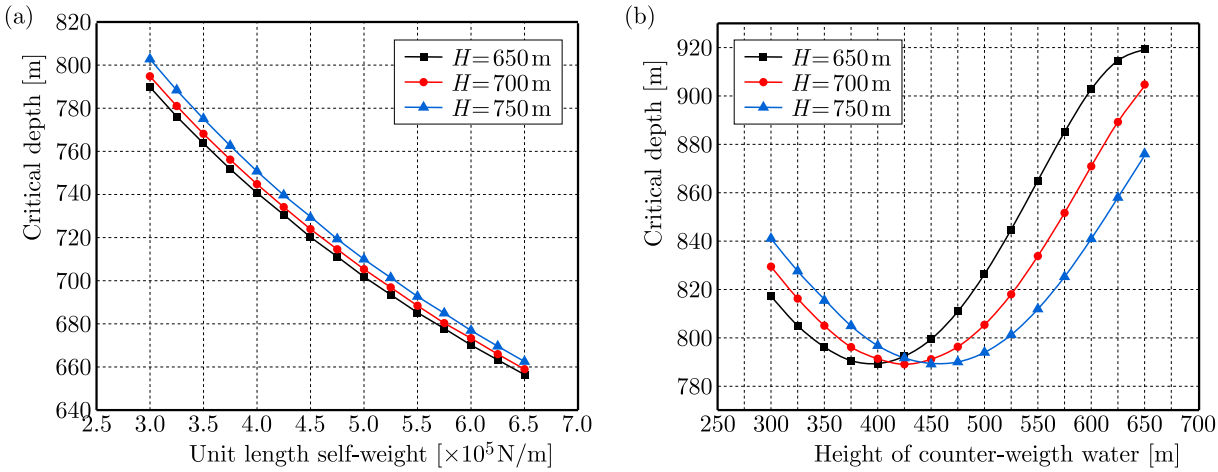

Fig. 5. Critical depth with different self-weights per unit length (a) height of counterweight water (b) at three construction heights

An additional study was carried out the to explore the relationship between critical depth and counterweight water height. When taking $D = 8\,\text{m}$, $d = 6.3\,\text{m}$, $E = 31.5\,\text{GPa}$, $p+c = 3\cdot10^5\,\text{N/m}$, the critical depth with different counterweight water heights is shown in Fig. 5b. The calculation results under three construction heights all show that the critical depth basically increases with the increase of counterweight water height, but there is a sudden change in the critical depth when counterweight water height reaches about 425 m. Critical depths for three counterweight water heights are all greater than construction height and the structure is vertically stable. It suggests that controlling counterweight water height within a reasonable range is favorable for ultra long DSLS.

Multifactor sensitivity analysis (Wang *et al.*, 2023) is a technique for assessing the effect of several uncertain elements changing simultaneously in a process. It can help one to analyze the effect of each factor on analytical indicators at various amplitudes, Figure 6 gives the calculation results of sensitivity coefficients for four influencing factors on the critical depth. The results reveal that factors described in order of the degree of influence are the inner diameter, elastic modulus, unit length self-weight, and counterweight water height sequentially. And the order of influencing factors forr three construction heights is exactly the same.

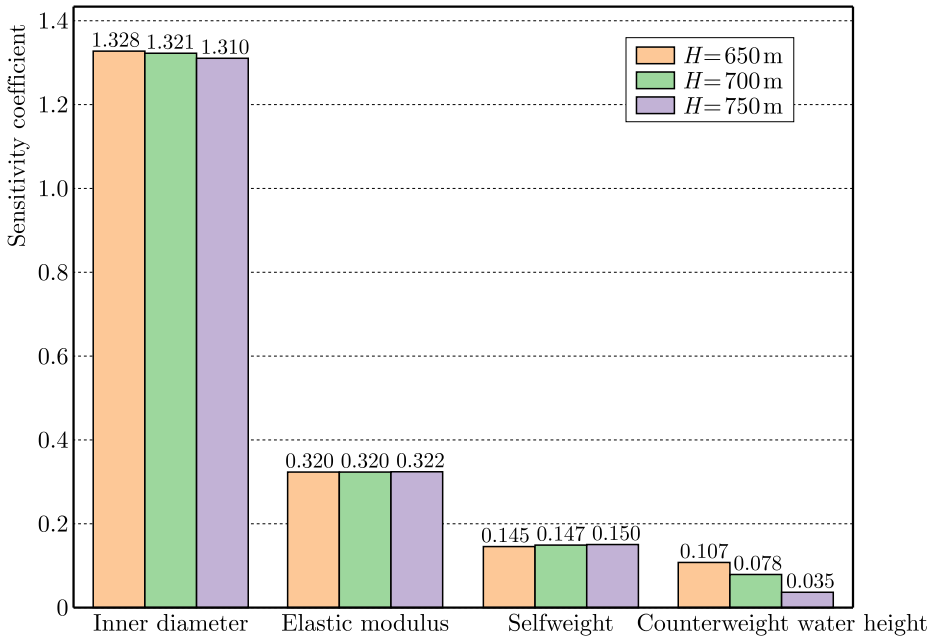

Fig. 6. Multi factor sensitivity analysis

4. Validation

4.1. Engineering background

North air shaft of Taohutu coal mine is located in the central eastern part of the Maowusu Desert in northeast China. The shaft is constructed by the drilling method, with a borehole diameter of 9.4 m, outer diameter of 8.1 m, minimum inner diameter of 6.5 m, total construction height of 751 m. Based on the engineering geological and hydrogeological conditions of the shaft passing through the strata, as well as the situation where the shaft will bear loads, it is determined that the DSLS adopts a combination of reinforced concrete shaft structure, double-layer inner and outer steel plates-reinforced concrete composite shaft structure. In the range of elevation $\pm 0 \sim -396$ and $-747 \sim -751$, a reinforced concrete shaft structure is used. Between $-396 \sim -747$, a double-layer steel plate reinforced concrete composite shaft structure is used. Concrete grade has a minimum strength of C40 and a maximum strength of C75.

4.2. Numerical validation

The parameters of shaft engineering are determined by calculation and normalization. The calculated parameters for the shaft elastic modulus, inner diameter and unit length self-weight are obtained by the ratio of cumulative sum of the product of each shaft section height and elastic modulus, inner diameter, or unit length self-weight to the total length of the shaft. So $E = 39.48$ GPa, $d = 6.8$ m, $p_c = 4.45 \cdot 10^5$ KN/m, $H_w = 423.8$ m. Following substituting into formula (3.2), the critical depth is 758 m when using the instability optimization measure. Due to the critical depth being greater than the total construction height, the shaft structure is stable. Theoretically, the shaft will not experience vertical instability after implementing the instability optimization measure. To further verify the effectiveness of instability optimization measure comparatively, we calculate the critical depth under traditional construction techniques according to literature in which the critical depth is also determined by cusp catastrophic model. It is found that the critical depth is 522.7 m, which is significantly smaller than the total construction height. So if traditional construction techniques are used, the shaft will experience vertical instability. Table 1 lists the comparison calculation results between the instability optimization measure and traditional techniques for Taohutu North air shaft.

As shown in Table 1, the critical depth found by using instability optimization measure is 1.45 times greater than that of traditional construction techniques. The critical depth of instability optimization measure increases by 45% compared to traditional construction techniques. It validates that the instability optimization measure effectively mitigates the instability of DSLS in Taohutu North air shaft.

Table 1. Comparison between instability optimization measure and traditional techniques for Taohutu North air shaft

	Instability optimization measure	Traditional construction techniques
Basis for critical depth calculation	Equation (3.2)	Liu *et al.* (2.20)
Critical depth calculation results	758 m	522.7 m
Instability criterion	$H < H_{cr}$	$H > H_{cr}$
Theoretical analysis conclusion	stable	unstable

5. Conclusion

By considering the characteristics of obvious suddenness and irreversible damage, the catastrophe method and cusp catastrophe model is employed to describe the instability process and mechanism of ultralong DSLS when applying the instability optimization measures. The following conclusions can be drawn from the numerical analysis:

- The cusp catastrophe model proposed in this paper can accurately describe the structural buckling behavior of ultralong DSLS under the instability optimization measure. The bifurcation set equation composed of control variables helped one to analyze the stability characteristics.
- The ultra long DSLS vertical instability and failure are the result of a gradual trend toward abrupt changes. Quantitative calculation of the critical depth helps one to evaluate stability of the shaft. Only when the critical depth reaches construction height, the shaft is in a critical stable condition.
- The critical depth of this instability optimization measure is dependent on the material properties and external factors. It decreases with increasing inner diameter and self-weight per unit length, and rises with increasing elastic model and counterweight water height. Lightweight and high-strength materials, as well as thick shaft structures are more popular in utilizing the instability optimization measure.
- Adopting instability optimization measure can increase the critical depth by approximately 45% compared to the traditional construction method. This instability optimization measure can theoretically mitigate the structural instability of DSLS, and its feasibility would be approved by more and more engineering.

Acknowledgement

This research was supported by Scientific Research Foundation for High-level Talents of Anhui University of Science and Technology (2024yjrc04).

References

1. Cheng H., Liu J.-M., Rong C.-X., Yao Z.-S., 2008, Variable cross section shaft drilling lining's vertical stability in thick alluvium, *Journal of China Coal Society*, **33**, 12, 1351-1357

2. Dorn E., Kaledin O., 2013, Modern and innovative shaft sinking and construction technology with examples from current projects/Moderne und innovative Schachtbautechnik am Beispiel aktueller Abteufprojekte, *Geomechanics and Tunnelling*, **6**, 5, 574-581

3. Fang Y., Yao Z., Xu Y., Li X., Liu X., Huang X., 2023, Permeability evolution and pore characteristics of reactive powder concrete of drilling shaft with initial salt erosion damage, *Construction and Building Materials*, **403**, 133141

4. Hara T., Yashima A., Sawada K., Kariya K., Tsuji H., Soga N., 2019, Small-diameter vertical shafts constructed in the shallow space of steep mountainous areas, *Underground Space*, **4**, 3, 235-250

5. Hong B.-Q., 1980, Axial stability of deep shaft wall in mud by drilling method, *Coal Science and Technology*, **9**, 22-25

6. Karman A., Pawlowski M., 2022, Circular economy competitiveness evaluation model based on the catastrophe progression method, *Journal of Environmental Management*, **303**, 114223

7. Lei Y., Li P.-J., Liu Z.-Y., Li J.-Z., Hu W., 2022, Method for calculation of buckling critical load of pile foundation crossing karst cave in karst area, *Rock and Soil Mechanics*, **43**, 3347-3356

8. Li Y., Tang N., Jiang X., 2016, Bayesian approaches for analyzing earthquake catastrophic risk, *Insurance: Mathematics and Economics*, **68**, 110-119

9. Liu J., Cheng H., Rong C., Wang C., 2020, Analysis of cusp catastrophic model for vertical stability of drilling shaft lining, *Advances in Civil Engineering*, **2020**, 1, 8891751

10. Liu J., Liu Y., Fu X., 2022, Mechanism analysis of catastrophic instability of drilling shaft lining based on Python language, *Coal Science and Technology*, **50**, 9, 75-81

11. Liu Z., Meng Y., 2015, Key technologies of drilling process with raise boring method, *Journal of Rock Mechanics and Geotechnical Engineering*, **7**, 4, 385-394

12. Merli M., Pavese A., 2018, Electron-density critical points analysis and catastrophe theory to forecast structure instability in periodic solids, *Acta Crystallographica. Section A: Foundation and Advances*, **74**, 102-111

13. Niu J.M., Wu J.H., Liu X.L., Yuan M.Q., Wang L.B., 2023, Quantitative analysis of acoustic black hole property by the catastrophe theory, *International Journal of Mechanical Sciences*, **259**, 108621

14. Niu X.-C., Hong B.-Q., Yang R.-S., 2006, Study on vertical structural stability of bored shafts filled part of water, *Rock and Soil Mechanics*, **27**, 1897-1901

15. Ozbasaran H., 2018, Optimal design of I-section beam-columns with stress, non-linear deflection and stability constraints, *Engineering Structure*, **171**, 385-394

16. Pacoste C., 1993, *On the Application of Catastrophe Theory to Stability Analyses of Elastic Structures*, Royal Institute of Technology, Stockholm

17. Saunders P.T., 1980, *An Introduction to Catastrophe Theory*, Cambridge University Press, Cambridge

18. Wang E., Zhang L., Chen H., Zhang X., 2023, Collinearity-oriented sensitivity analysis for patterning energy factor significance in buildings, *Journal of Building Engineering*, **73**, 106685

19. Wegner T., Kurpisz D., 2017, An energy-based method in phenomenological description of mechanical properties of nonlinear materials under plane stress, *Journal of Theoretical and Applied Mechanics*, **55**, 1, 129-139

20. Xing X., Ma B., Du J., Liu Y., Liu Z., Han X., 2023, An energy method for predicting and suppressing the instability of a three-dimensional thermoacoustic coupling system with a microperforated plate, *Journal of Theoretical and Applied Mechanics*, **61**, 4, 755-768

21. Xu J., Ni Y., 2019, Prediction of grey-catastrophe destabilization time of a granite residual soil slope under rainfall, *Bulletin of Engineering Geology and the Environment*, **78**, 5687-5693

22. Yang S., 2019, Influence analysis of buckling stability of super-long piles under different working conditions based on energy method, Master's Thesis, China University of Geosciences, Wuhan, China

23. Zhao K., Wu J., Yan Y., Yang J., Tian X., *et al.*, 2023, The cusp catastrophe warning model for easily weathered granite considering energy accumulation and dissipation, *Environmental Science and Pollution Research*, **30**, 45888-45898

Manuscript received February 3, 2024; accepted for publication September 30, 2024